Research Article | Vol. 29, No. 26 / 20 Dec 2021 / Optics Express 42713
Optics EXPRESS

Terahertz polarizer based on tunable surface plasmon in graphene nanoribbon

DIP SARKER,[1,3] PARTHA PRATIM NAKTI,[1,3] MD ISHFAK TAHMID,[1,2] MD ASADUZ ZAMAN MAMUN,[1] AND AHMED ZUBAIR[2,*]

[1]*Department of Electrical and Electronic Engineering, Shahjalal University of Science and Technology, Sylhet 3114, Bangladesh*
[2]*Department of Electrical and Electronic Engineering, Bangladesh University of Engineering and Technology, Dhaka, Bangladesh*
[3]*These authors contributed equally to this work*
[*]*ahmedzubair@eee.buet.ac.bd*

Abstract: Tunable surface plasmon resonance-based graphene nanoribbon (GNR) terahertz (THz) polarizers with adjustable operating frequency are proposed in this work. While conventional THz polarizers lack robustness and tunability, recently reported graphene-based metastructure polarizers have complex fabrication processes and comparatively smaller extinction ratios (ERs). A comprehensive study using finite-difference time-domain (FDTD) simulation technique reveals high ER, broad tunability, near-perfect degree of polarization (DOP), and low insertion loss for our proposed single and double stage GNR polarizers. The operating frequency of these narrow band polarizers can be tuned by varying GNR width, GNR pitch, chemical potential, and substrate material. Our optimized THz polarizer has an ER of 30 dB which is comparable to the commercially available THz polarizers. The maximum insertion losses within the tunable frequency range were found to be 0.24 dB and 1.87 dB for single and double stage GNR polarizers, respectively, which are substantially low. We compared the performance of the proposed structures with recently demonstrated graphene-based metastructure polarizers. The polarizers are promising for the design of photonic devices, integrated photonic circuits, and optoelectronic systems.

1. Introduction

The collective oscillation of free electron gas density interacts with incident light in a surface plasmon-based polarizer. This polarizer attenuates undesired polarization states and only enables electromagnetic waves of a specific polarization to pass through. A wide range of applications, including contrast improvement display filters, sunlight readable touch screens, polarization converters, selective polarization devices and stress monitoring of glass and plastics, piqued the interest of researchers in exploring polarizers [1–6]. Consequently, substantial theoretical and experimental work is conducted to build polarizers with superior performance such as wire grid polarizers and Glan-Tylor prism based polarizers. Deng *et al*. [7] and Huang *et al*. [8] suggested wire grid polarizers with high extinction ratios (ERs) and low losses. However, the production of such complicated structures is limited. Mao *et al*. [9] presented a high ER multilayer metal grating based polarizer that had a challenging construction procedure. Although 1D extreme anisotropy of carbon nanotube was utilized to fabricate polarizers, their performance is limited by substantial insertion loss [10]. Alternative structures based on metamaterials were proposed to enable efficient modulation of terahertz polarization [11]. However, fixed structural factors restrict adjusting of resonant frequency in such devices. There is scope for further research to develop a tunable, high ER, and low loss polarizer with simple fabrication process.

#444706 https://doi.org/10.1364/OE.444706
Journal © 2021 Received 1 Oct 2021; revised 24 Nov 2021; accepted 29 Nov 2021; published 8 Dec 2021

Optics EXPRESS

Graphene, a highly conductive carbon material, has long-lived plasmon excitation, excellent low-loss properties, and adjustable characteristics. These features make graphene a favorable material for plasmonic devices. Due to its tunable plasmonic nature, resonant frequency may be adjusted by changing structural parameters such as width, pitch, substrate and by using voltage source. Several graphene-based polarizers have already been explored in a wide frequency range from GHz to THz. Arab *et al*. described a textured graphene structure capable of providing 10 dB - 22 dB ER that is difficult to fabricate due to its intricate textured nature [12]. Meng *et al*. [13] has previously reported a maximum of 30 dB ER in the THz frequency regime. There is a scope for significant performance improvement of graphene-based polarizer structures.

In this paper, we proposed two graphene nanoribbon based THz polarizers with low insertion loss, broad tunability, and high ER. The performance parameters of the device were analyzed using finite-difference time-domain (FDTD) simulation technique. The graphene nanoribbon array on silicon substrate passes the light through the structure to get desired transmission transverse magnetic (TM) and block the remaining one transverse electric (TE). ER was found to be 16 dB to 24 dB for the operating frequency of 1.81 THz to 3.75 THz by our proposed single stage GNR polarizer. Furthermore, we proposed a double stage GNR polarizer with improved performance that provides an ER up to 30 dB at 3.81 THz. Tuning can be accomplished by changing structural parameters such as GNR width, pitch and substrate, and the chemical potential of the graphene layer with the help of a voltage source. The high electron mobility of graphene also allows to vary scattering rates for controlling the sharpness of the peak of transmission spectra. Moreover, we proposed a straightforward fabrication method for manufacturing the THz polarizers.

2. Device structure and methodology

The structure of the proposed THz polarizer is comprised of periodically patterned monolayer graphene, which is made up of GNR patterns, on a Si substrate as depicted in Fig. 1(a). Figure 1(b) illustrates a schematic representation of the polarizer's unit cell. Substrate height (h) is set at 2 μm to avoid Fabry-Perot multi-reflections [14]. A periodic arrangement of airstrips in graphene layer makes up the GNR array on the top surface. The GNR has a width, w of 10 nm and a pitch, d of 20 nm for the designed structure. The unit cell's overall length and width (both denoted by p) were set to 3 μm, while the GNR array length, l was set to 2.5 μm.

The surface conductivity of graphene is modeled by the well-known Kubo's formulation [15],

$$\sigma(\omega, \Gamma, \mu_c, T) = \sigma_{inter}(\omega, \Gamma, \mu_c, T) + \sigma_{intra}(\omega, \Gamma, \mu_c, T), \tag{1}$$

$$\sigma_{intra}(\omega, \Gamma, \mu_c, T) = \frac{-ie^2}{\pi\hbar^2(\omega + i2\Gamma)} \int_0^\infty \xi\left(\frac{f_d(\xi)}{\partial\xi} - \frac{\partial f_d(-\xi)}{\partial\xi}\right) d\xi, \tag{2}$$

$$\sigma_{inter}(\omega, \Gamma, \mu_c, T) = \frac{ie^2(\omega + i2\omega\Gamma)}{\pi\hbar^2} \int_0^\infty \xi\left(\frac{f_d(-\xi)}{(\omega + i2\Gamma)^2} - \frac{f_d(\xi)}{4(\xi/\hbar)^2}\right) d\xi, \tag{3}$$

$$where, f_d(\xi) = \frac{1}{exp((\xi - \mu_c)/(k_B T)) + 1}. \tag{4}$$

Here, e denotes the electron charge, ω is the angular frequency, $\hbar$ is the reduced Planck's constant, T is the temperature, and Γ is the scattering rate. μ_c, f_d, and ξ represent the chemical potential, the Fermi-Dirac distribution function, and the energy, respectively. Total conductivity is the sum of intraband (σ_{intra}) and interband (σ_{inter}) terms. Though the model is specifically designed for surface conductivity of single layer graphene, it may also be expanded to describe multilayer graphene conductivity [16,17].

To create a improved design of polarizer, we used a double stage graphene layer structure, one on top and another at the bottom surface of the substrate. Schematic representation of a unit cell

Optics EXPRESS

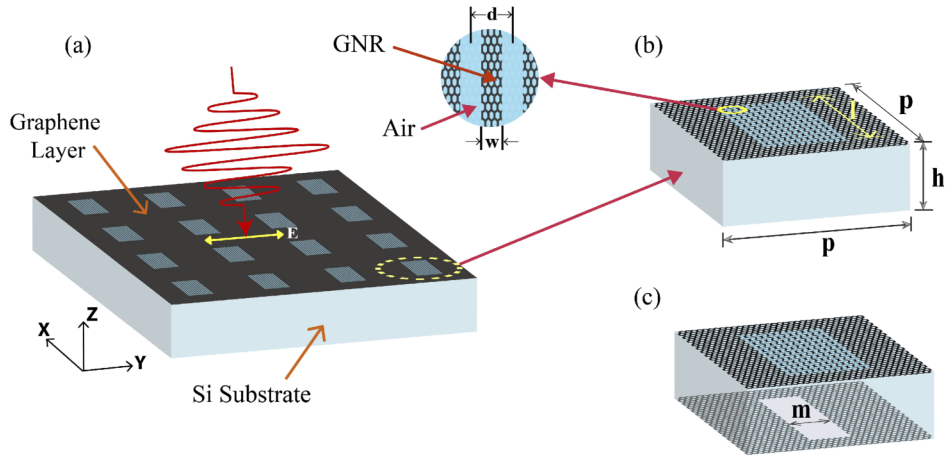

Fig. 1. (a) Three dimensional schematic view of the proposed polarizer structure under normal incident of THz wave with electric field along y direction. (b) A unit cell of single stage GNR polarizer with geometrical parameters: d = 20 nm, w = 10 nm, l = 2.5 μm, p = 3 μm and h = 2 μm. (c) Unit cell of double stage GNR polarizer. There are graphene layer on both side of the Si substrate with structural parameters: p = h = 2 μm, l = 2.5 μm, m = 150 nm, d = 20 nm, w = 10 nm.

of double stage GNR polarizer is shown in Fig. 1(c). The top layer is similar to that of the single stage design. However, the bottom graphene layer was made up of a single rectangular air hole with a width, m of 150 nm. Here, the chemical potentials of the top and the bottom graphene layers are designated by μ_{c_1} and μ_{c_2}, respectively and the rest of the parameters are kept identical to those of single stage GNR polarizer. The performance were quantitatively analyzed using the 3D FDTD analysis method. In the x and y directions, periodic boundary conditions were used, while the steep angle perfectly matched layer (PML) boundary condition was used in the positive and negative z-direction. Non-uniform conformal mesh was considered for our simulation. To prevent light reflection from the PML border, the thickness of the PML layer was designed to be higher than the peak wavelength of the source. Plane wave light source with a central frequency of 3 THz was incident from the top along negative z direction and the transmission spectra was recorded by a power monitor at the bottom of the cell.

3. Proposed fabrication process

Graphene materials can be produced via chemical vapor deposition (CVD). In addition, this process can be used to make monolayer graphene on a silicon substrate. Metal-free, ambient pressure CVD can produce graphene directly on both sides of a single-crystal silicon substrate [18] as shown in Fig. 2. The nanoribbons in our polarizer design can be created precisely by patterning CVD grown monolayer graphene using the helium ion beam lithography (HIBL) due to its reduced beam spot size and comparatively short scattering length. HIBL has the capability to fabricate tunable width, aligned and very high resolution GNR arrays [19]. Similarly, the air hole in the bottom graphene monolayer can be created using photolithography or HIBL technology as can be seen in Fig. 2 [20]. Additionally, we can use electron beam lithography and oxygen plasma etching techniques to pattern nanoribbon as narrow as 10 nm [21].

Optics EXPRESS

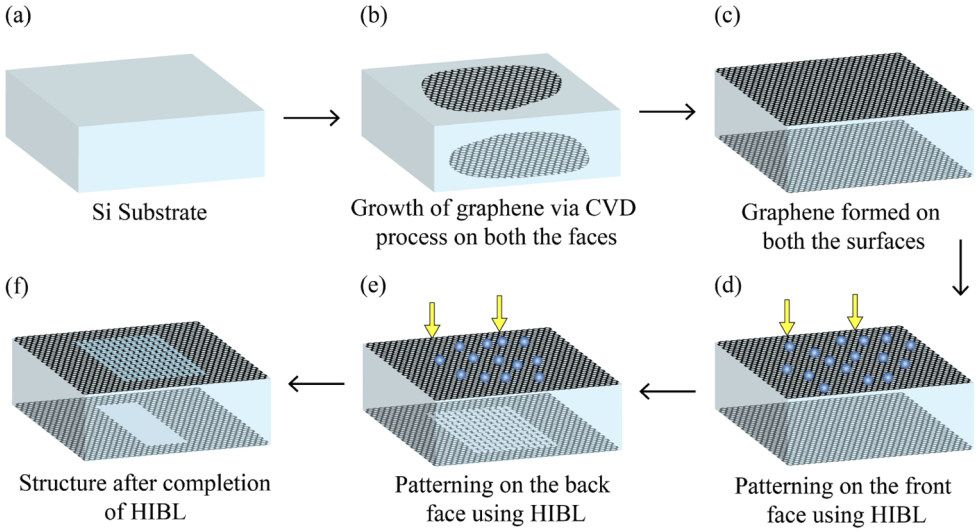

Fig. 2. Scheme of the fabrication process of the proposed polarizer. (a) Schematic of Silicon substrate. (b) Graphene is grown on both the faces of silicon using metal-free CVD process. (c) View after formation of graphene on Silicon. (d) Patterned GNR using HIBL process on the top surface of silicon. (e) Patterned GNR using HIBL process on the bottom surface of silicon. (f) View after patterning GNR on both the sides of silicon.

4. Results and discussion

4.1. Single stage GNR polarizer

Incoming photons of a certain energy interact with the plasmon in GNR array, resulting in surface plasmon resonance (SPR). As a consequence, photons are attenuated at the structure's top surface, and less light is transferred to the transmission monitor. The intensity of this interaction in our design is determined by the electric field direction of the incoming light. As shown in Fig. 3(a), our suggested structure transmits transverse magnetic (TM) light, while attenuating transverse electric (TE) light at 3.75 THz. For this case, chemical potential, μ_c was 0.9 eV, relaxation time, τ was 2 ps, and other structural parameters were mentioned before. The reflectance and absorption spectra for both TE and TM incident THz light are presented in Supplement 1.

As evident from the electric field distribution of Figs. 3(c) and 3(d), strong resonance at 3.75 THz frequency prevents the transmission of light for TE polarization, and TM polarized light passes through the structure at resonant frequency. A performance parameter of polarizer, extinction ratio (ER) is defined by,

$$ER = 10log_{10}(\frac{T_{TM}}{T_{TE}}). \tag{5}$$

where T_{TM} and T_{TE} are the transmittance for TM and TE polarized incident light, respectively. Resulting ER for our proposed polarizer is presented in Fig. 3(b) and it is found to be 24 dB at 3.75 THz.

To evaluate the impact of incident light polarization angle on device performance, we examined the transmittance spectra at various polarization angles. According to Malus's law, the intensity of transmitted polarized light is proportional to the square of the cosine of the polarization angle (φ) of incident light, and mathematically given by,

$$I \propto cos^2(\varphi). \tag{6}$$

Optics EXPRESS

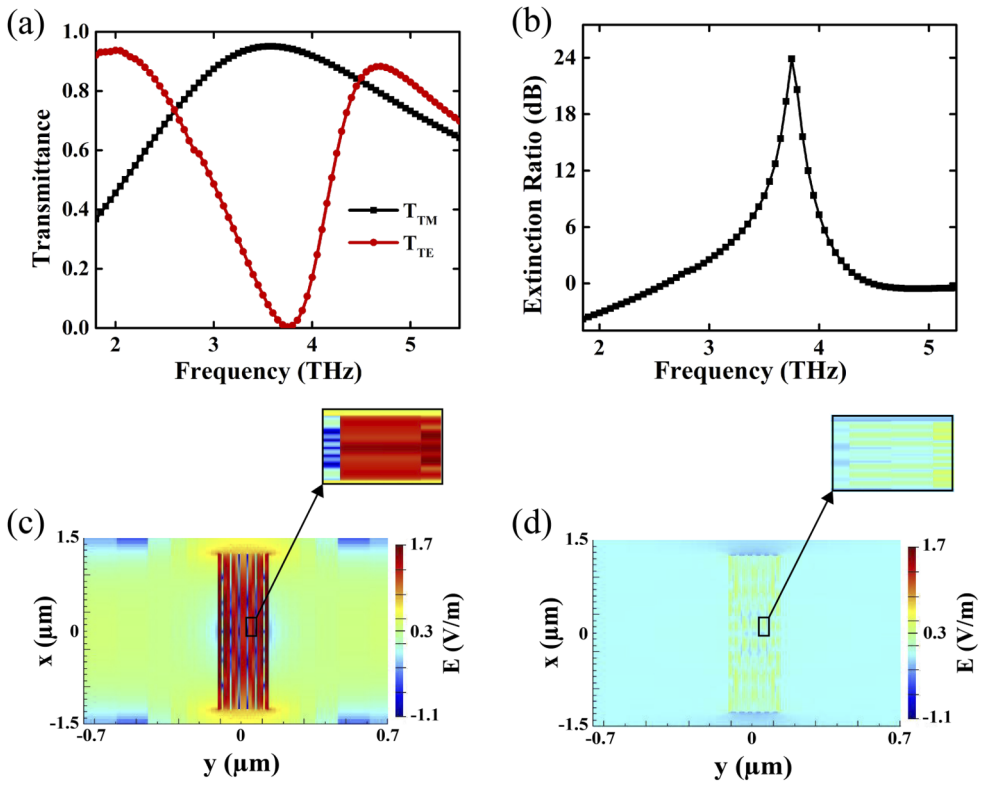

Fig. 3. (a) Transmittance spectra of TM polarization (black line with black square marker), and TE polarization (red line with red circular marker) for single stage GNR polarizer. (b) Extinction ratio of single stage polarizer for 0.9 eV chemical potential. (c) Spatial electric field distribution for TE polarized incident light on the polarizer at 3.75 THz. To demonstrate the presence of interaction of plasmons between two nanoribbons, magnified view of electric field is shown in inset. (d) Spatial electric field distribution for TM polarized incident light on the polarizer at 3.75 THz. To demonstrate the interaction of plasmons between two nanoribbons, magnified electric field is shown in inset.

Here, I denotes the intensity of polarized light after transmission. As evident from Fig. 4(a), transmission intensity is minimum for $\varphi = 90°$ (TE mode) and maximum for $\varphi = 0°$ (TM mode), which corroborate with Eq. (6). Transmission of light varies following the Malus's law as expected.

The polar plot of normalized transmission is shown in Fig. 4(b). We observed a polarization-dependent THz transmission with lowest transmission for the TE polarization and highest transmission for the TM polarization. It is evident from the time domain waveforms of transmitted THz electric field that TE polarized light undergoes significant modification (See Fig. S2 of Supplement 1).

To explore the tuning characteristics, the resonant frequency is adjusted in two ways: (i) modifying structure and (ii) changing the chemical potential of GNR layer using voltage source. The structure was modified by varying GNR width (w), pitch distance (d), and substrate. In addition to changing resonant frequency via modifying structure, it can be possible to change resonant frequency and optical properties using micro-electromechanical devices [22,23]. The change of the GNR's resonant frequency (ω_p) with w and chemical potential (μ_c) follows the

Optics EXPRESS

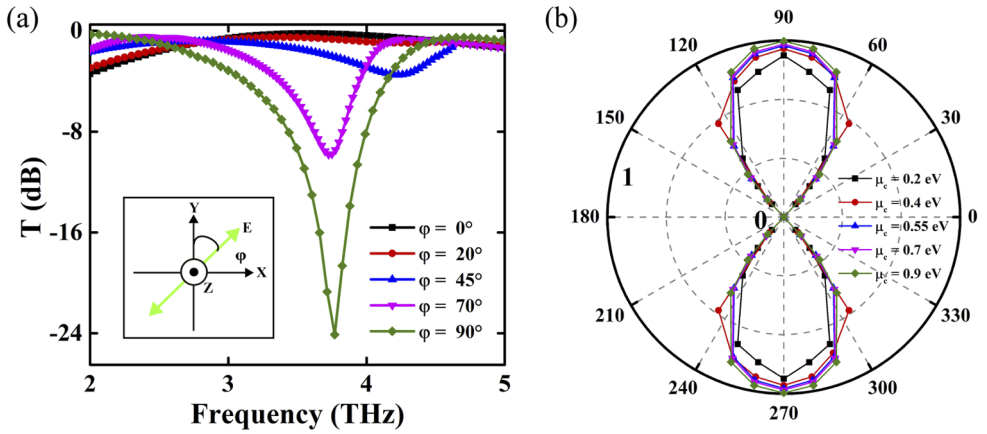

Fig. 4. (a) Transmission spectra of single stage GNR polarizer for varying incident light polarization angle, φ. Here, chemical potential was considered to be 0.9 eV, and relaxation time was 2 ps. Inset shows the direction of electric field which is assumed to be plane wave. (b) Normalized transmission $(T_{TM} - T_{TE})/T_{TM}$ of the THz polarizer for 0.2 eV (black line with square marker), 0.4 eV (red line with circle marker), 0.55 eV (blue line with triangle marker), 0.7 eV (pink line with inverse triangle marker), and 0.9 eV (green line with diamond marker) chemical potential. In this polar plot, the polarization angle is defined with respect to TE polarization.

scaling laws given in Eq. (7) [24,25].

$$\omega_p \propto \frac{1}{\sqrt{\mathrm{w}}} \propto |\mu_c|^{\frac{1}{2}}. \tag{7}$$

According to this relation, an increase in w decreases the resonant frequency, which is also evident from the transmittance spectra of Fig. 5(b). As apparent from Figs. 5(a) and (b), changes in the distance between nanoribbon (d) provides superior tuning capabilities compared to changes in the width of GNR (w). While the former can tune the resonant frequency from 3.75 THz to 4.28 THz for a variation in d from 20 nm to 50 nm, a trifle change in the resonant frequency in the range 3.7 THz to 3.8 THz for the later is observed for variation of w from 5 nm to 15 nm. It is also noteworthy that resonant frequency blueshifts for increasing d. However, it redshifts for increasing w. If w is much wider or narrower, then the interaction of graphene with surface plasmons is minimized. Hence, particular attention should be given while changing w. Otherwise, ER of the polarizer will degrade.

To tune the resonant frequency without any structural modification, we varied the μ_c of GNR layer, which is given by [24],

$$\mu_c \approx \hbar v_f \sqrt{\frac{\pi \in_r \in_0 V_g}{e\tau}}. \tag{8}$$

where, V_g represents the external bias voltage, v_f is the fermi velocity, τ is the relaxation time, $\in_r$ is the relative permittivity of the substrate and, $\in_0$ is the permittivity of the vacuum. By changing the μ_c of Graphene using an external voltage source as shown in the inset of Fig. 6(a), resonant frequency can be controlled. As can be seen in Fig. 6(a), the resonant frequency can be widely tuned from 2.5 THz to 3.75 THz by changing chemical potential from 0.4 eV to 0.9 eV. The peak of resonant also gets higher for larger value of chemical potential. This happens due to the greater charge accumulation for μ_c = 0.9 eV than that for smaller values of μ_c. Thus, ER can be enhanced significantly by increasing the chemical potential of the graphene layer.

Optics EXPRESS

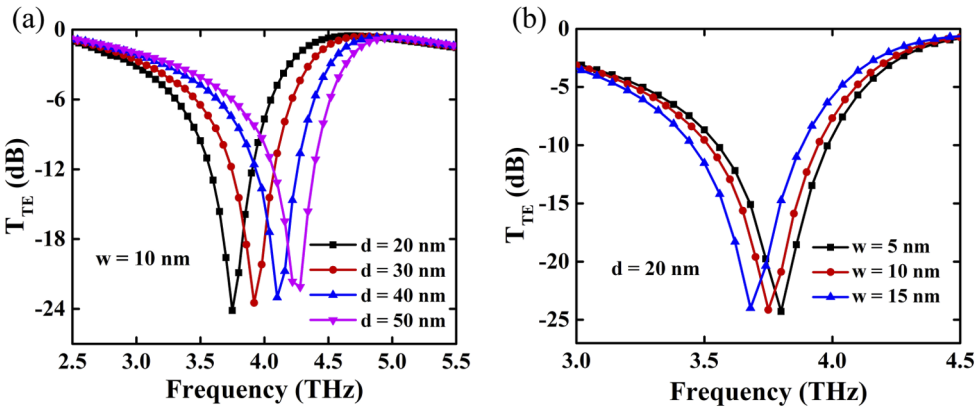

Fig. 5. (a) Transmission spectra of single stage GNR polarizer for different values of d considering w = 10 nm, μ_c = 0.9 eV, and τ = 2 ps. (b) Transmission spectra for different values of w assuming d = 20 nm, μ_c = 0.9 eV, and τ = 2 ps.

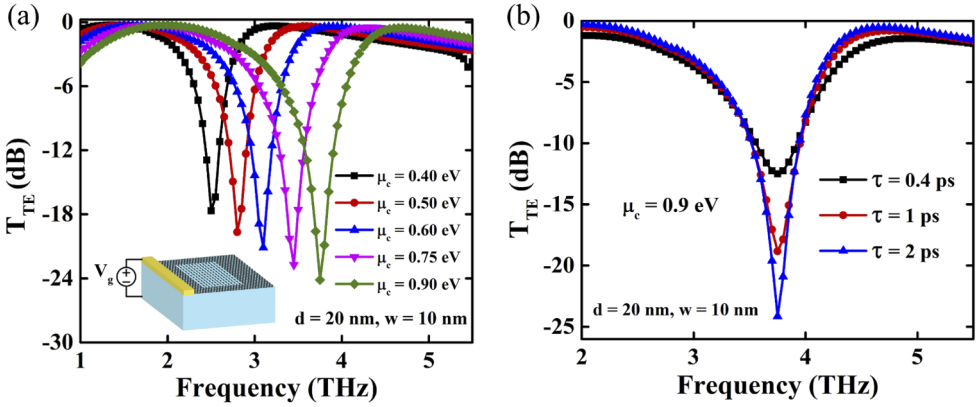

Fig. 6. (a) Transmission spectra of single stage GNR polarizer for different values of μ_c with τ = 2 ps. Illustration of the experimental setup for varying μ_c is provided in the inset. (b) Transmission spectra of single stage GNR polarizer for different values of τ assuming μ_c = 0.9 eV. We considered d = 20 nm, and w = 10 nm.

The damping ratio, Y can be given by [26],

$$\mathrm{Y} = 2\hbar\Gamma = \frac{\hbar}{\tau}, \tag{9}$$

Moreover, Y can also be defined as,

$$\mathrm{Y} = \frac{e\hbar v_f^2}{\mu\mu_c}. \tag{10}$$

Here, Γ is the scattering rate, and μ is the mobility of the GNR layer. Comparing Eq. (9) and Eq. (10), we can write "$\tau \propto \mu$". According to this relation, lower mobility corresponds to less mobile plasmons, which do not interact on the surface appropriately. As a result, higher loss and lower intrinsic quality factor, Q occur. Thus, the transmission spectra's notches become broader and shallower for lower value of τ, which is evident in Fig. 6(b). From the above discussion, it can be inferred that sharp and dominant peak can be obtained with higher chemical potential along with a higher relaxation time. Consequently, the maximum ER for our study was found

Optics EXPRESS

with chemical potential and scattering time of 0.9 eV and 2 ps, respectively. Corresponding ER was found to be 24 dB, which is shown in Fig. 3(b).

Additionally, we investigated the impact of various substrate on the resonant frequency. Different substrates influence the interaction between it and the graphene layer. As a consequence, SPR occurs at different frequencies for different substrates. As apparent from Fig. 7, resonant frequency can be adjusted from roughly 3.75 THz to 7.25 THz by changing the substrate. The substrates considered in our study were Si, GaAs, GaP, and PMMA. Among the substrate considered, Si offers the lowest (3.75 THz) and PMMA offers the highest (7.25 THz) resonant frequency.

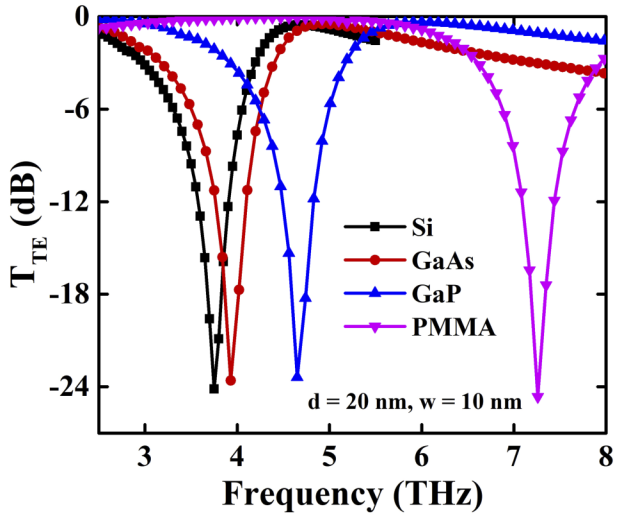

Fig. 7. Transmission spectra of single stage GNR polarizer for different substrate materials considering μ_c = 0.9 eV, and τ = 2 ps.

4.2. *Double stage GNR polarizer*

The surface conductivity of graphene in a double stage GNR structure is greater than that of a single stage GNR structure. Hence, the transmittance is much smaller at that resonant frequency. The full width half maximum (FWHM) of the resonance peak is 80 GHz for single stage GNR polarizer. It is evident from Fig. 8(a) that when chemical potentials of top (μ_{c_1}) and bottom (μ_{c_2}) GNR layers both are at 0.4 eV or 0.9 eV, we obtain a deeper dip at the resonant frequency than the single layer arrangement. When $\mu_{c_1} = \mu_{c_2}$ = 0.4 eV (black line), the FWHM is ~ 200 GHz, and when $\mu_{c_1} = \mu_{c_2}$ = 0.9 eV (red line), the FWHM is ~ 170 GHz, as illustrated in Fig. 8(a). When two separate chemical potential is employed concurrently in top and bottom layers, two unique resonant peaks were observed. This phenomenon can be described using the idea of plasmon induced transparency (PIT). The idea of PIT really originates from electromagnetically induced transparency (EIT). PIT has two modes in the plasmonic study: bright mode (super-radiant) couples strongly with incident light, and dark mode (sub radiant) pairs weakly with incident light [27–32]. A dark mode occurs in between two bright modes. We utilized surface plasmon polariton (SPP) coupling of top and bottom GNR layers which results in two bright modes and a weak hybridization in between them that produces a narrow transmission window as illustrated in Fig. 8(a). For this case, the PIT was created by using chemical potentials of μ_{c_1} = 0.9 eV and μ_{c_2} = 0.4 eV at top and bottom surfaces, respectively. Figure 8(b) shows the simulated transmission spectra with different values of μ_{c_1} and μ_{c_2}.

Optics EXPRESS

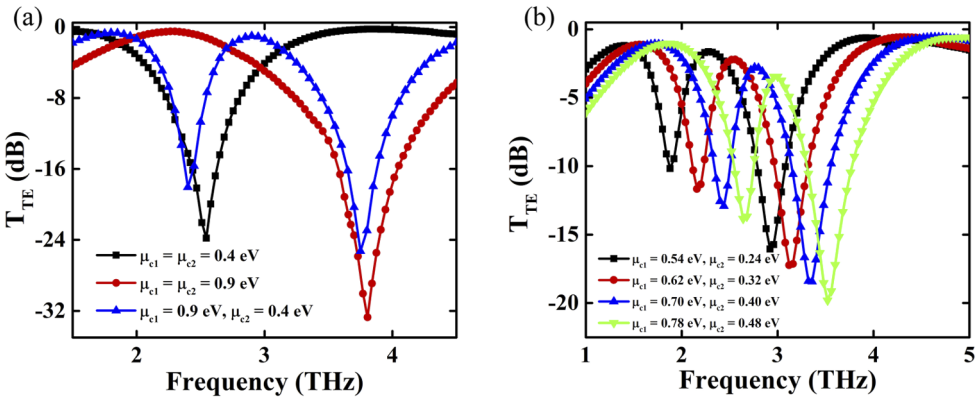

Fig. 8. (a) Transmission spectra of double stage GNR polarizer for same and different chemical potentials at top and bottom GNR layers. (b) Transmission spectra using different values of μ_{c_1} and μ_{c_2} for double stage GNR polarizer.

Dual resonance frequency points and narrow transparency regions shift with varying chemical potentials, and narrow transparency windows are at 2.3 THz for $\mu_{c_1} = 0.54$ eV and $\mu_{c_2} = 0.24$ eV, 2.55 THz for $\mu_{c_1} = 0.62$ eV and $\mu_{c_2} = 0.32$ eV, 2.8 THz for $\mu_{c_1} = 0.7$ eV and $\mu_{c_2} = 0.4$ eV, 2.95 THz for $\mu_{c_1} = 0.78$ eV and $\mu_{c_2} = 0.48$ eV. ER of double stage GNR polarizer was found to be 30 dB for $\mu_{c_1} = \mu_{c_2} = 0.9$ eV. The reflectance and absorption spectra of double stage GNR polarizer for both TE and TM incident THz light are presented in Supplement 1.

For better understanding of this phenomenon, the electric field distribution for 2.4 THz and 3.75 THz at the top and bottom surfaces are shown in Fig. 9. At 2.4 THz, the top layer attenuates a part of the incoming light and the remaining transmitted light interacts with the bottom layer. As a consequence, the resonance's intensity is reduced. However, the incoming light interacts with the GNR array on the top surface at 3.75 THz resulting in a resonance. The resonance peak at this frequency is more pronounced. Due to the GNR array, plasmon interaction with the light in the top graphene layer is much significant compared to that in the bottom graphene layer. Consequently, the combined effect of the plasmon interaction with light at the two graphene layers produces two different transmission dips at resonant frequencies.

4.3. Performance analysis

If light is represented by Stokes vectors, optical sample can be described by a real-valued 4x4 matrix that is called Mueller Matrix. We calculated Mueller matrices for our proposed THz polarizers. The significant elements of Mueller matrix are given by [33],

$$m_{12} = \frac{T_{TM}^2 - T_{TE}^2}{2}, \tag{11}$$

$$m_{22} = \frac{T_{TM}^2 + T_{TE}^2}{2}, \text{and} \tag{12}$$

$$m_{33} = T_{TM} T_{TE}. \tag{13}$$

Here, m_{ij} being the ij-th element of Mueller matrix, i is the row number, and j is the column number.

The elements of the Mueller matrix for single stage GNR and double stage GNR polarizers are presented in Fig. 10. If we assume that the transmission axis of an ideal polarizer is in TM polarization direction, then $T_{TM} = 1$ and $T_{TE} = 0$ and the values of Mueller matrices are m_{12}

Optics EXPRESS

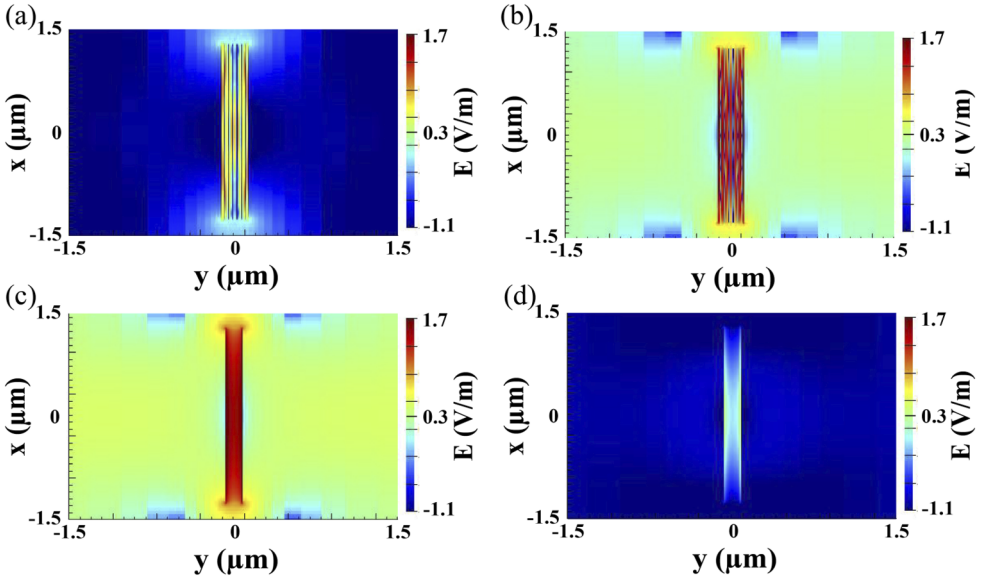

Fig. 9. (a) Electric field distribution of top Graphene surface with 0.9 eV chemical potential at 2.4 THz in double stage GNR polarizer. (b) Electric field distribution of top Graphene surface with 0.9 eV chemical potential at 3.75 THz in double stage GNR polarizer. (c) Electric field distribution of bottom Graphene surface with 0.4 eV chemical potential at 2.4 THz in double stage GNR polarizer. (d) Electric field distribution of bottom Graphene surface with 0.4 eV chemical potential at 3.75 THz in double stage GNR polarizer.

= 0.5, m_{22} = 0.5, m_{33} = 0 (black dot line). In comparison to an ideal polarizer, we achieved comparable results in our proposed THz polarizers. Nevertheless, the values of double GNR are considerably closer to the ideal than single GNR, as shown in Fig. 10.

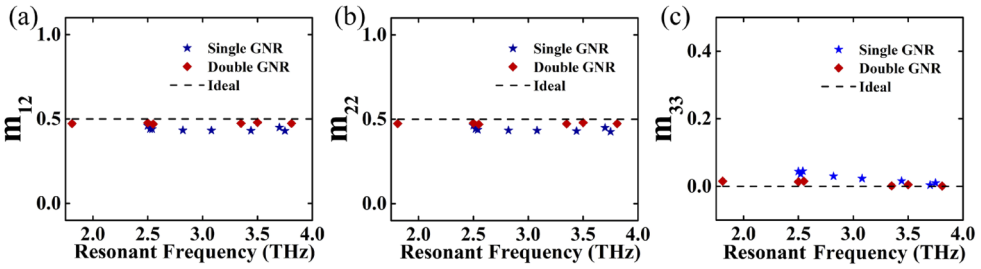

Fig. 10. Elements of Mueller matrix (a) m_{12}, (b) m_{22}, (c) m_{33} for single stage GNR polarizer (blue stars) and double stage GNR polarizer (red squares) w.r.t. ideal polarizer (black dot line).

An important polarizer performance parameter is insertion loss which is given by $-10log(T_{TM})$ in dB. We calculated the insertion loss as a function of resonant frequency for single and double stage GNR polarizers as shown in Fig. 11(a). It can be observed that our structure's insertion loss is within the range of 0.15 dB to 0.24 dB for single stage GNR polarizer and 0.83 dB to 1.87 dB for double stage GNR polarizer. Additionally, We calculated degree of polarization (DOP) given by,

$$\text{DOP} = \frac{T_{TM} - T_{TE}}{T_{TM} + T_{TE}}. \tag{14}$$

Optics EXPRESS

for single and double stage polarizers shown in Fig. 11(b). We achieved near-perfect DOP: between 95% to 99.3% for single stage GNR polarizer and 96.4% to 99.9% for double stage GNR polarizer at 1.8 THz to 3.8 THz resonant frequency.

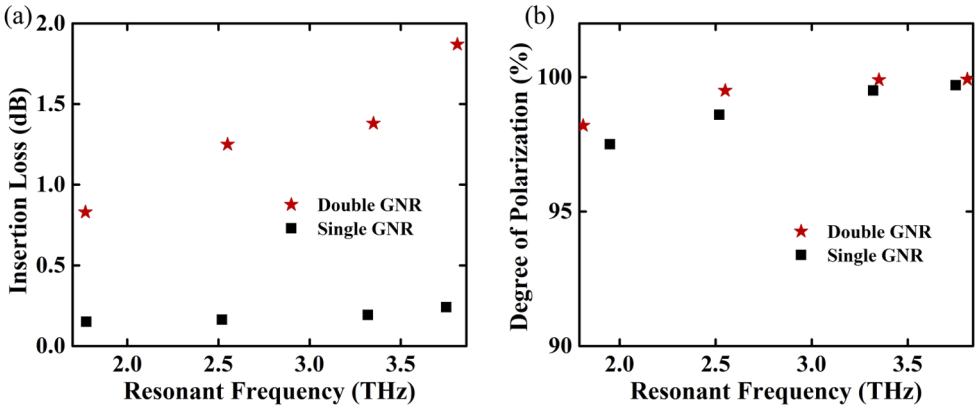

Fig. 11. (a) Calculated insertion loss as a function of resonant frequency for single stage GNR polarizer (black square marker) and double stage GNR polarizer (red star marker). (b) Measured degree of polarization (DOP) as a function of resonant frequency for single GNR stage polarizer and double stage GNR polarizer.

4.4. Comparative analysis

Table 1 shows a comparison of the performance parameters of our proposed polarizers with those of previously reported works. Meng *et al*. [13] reported a wire grid graphene polarizer that had an ER of up to 30 dB, which is comparable to us. However, wire grid graphene manufacturing method is considerably complicated. A textured multi-layer graphene grating based polarizer was reported by Arab *et al*. that had an ER of 10-22 dB over a frequency range similar to us [12]. The broadband graphene polarizer introduced by Bao *et al*. [34] is a single mode fiber with a small numerical aperture, making light coupling difficult. As a consequence, it has a minimum insertion loss of 5 dB. Pei *et al*. [35] was able to minimize the coupling issue by employing a waveguide polarizer. However, the insertion loss was considerably greater, reaching

Table 1. Performance of our GNR based Polarizers

Structure	Operating Frequency (THz)	Optical Bandwidth (THz)	DOP (%)	Insertion loss (dB)	ER (dB)	Reference
Wire grid graphene metal hybrid metasurfaces	0.2-2.5	3	99.7	2.54	Up to 30	[13]
Broadband graphene polarizer	193.5	–	99.6	5	27	[34]
Graphene/glass hybrid waveguide	219	–	99.6	9	28	[35]
Textured Graphene gratings	0.001-4	0.65	97.6	2.22	10-22	[12]
Proposed single stage GNR polarizer	1-4	0.08	95-99.3	0.15-0.24	Up to 24	This work
Proposed double stage GNR polarizer	1-4	0.17	96.4-99.9	0.83-1.87	Up to 30	This work

Optics EXPRESS

a maximum of 9 dB, while we had an insertion loss of 1.87 dB for maximum ER of 30 dB. We also achieved a near-perfect value of DOP. We suggested a simplified structure that is straight forward to fabricate. In comparison to existing single and double band polarizers, our suggested single band and double band polarizers offer higher ER. The operating frequency, which is the tunability range for our polarizers along with other relevant articles are shown in Table 1. The operating bandwidth of these structures is also depicted in Table 1.

5. Conclusion

In this study, surface plasmon resonance based GNR polarizers with low insertion loss, broad tunability, near-perfect DOP, and high ER in terahertz regime was reported. Interaction between light and plasmon in GNR layer results in resonance at certain frequency. Consequently, high attenuation occurs for light with specific polarization at resonant frequency. From the frequency response analysis of GNR on silicon substrate, the GNR width, pitch, substrate modification result in a resonant frequency shift. Although these structural parameters of our polarizers are nonadjustable after fabrication, tuning of resonant frequency is achievable by varying chemical potential of the graphene layer. We obtained a substantial enhancement in performance for double stage GNR polarizer compared to single stage GNR polarizer. Though insertion loss was marginally higher, our designed double stage GNR polarizer had 20% higher ER, and more than twice bandwidths compared to single stage GNR polarizer. Our proposed GNR polarizers are tunable from 1.8 to 3.8 THz. Our proposed terahertz polarizers, despite of their simple fabrication process, can be tuned in a wide terahertz range and can exhibit high ER with extraordinarily low insertion loss and high DOP. Hence, these terahertz polarizers will be functional in promising applications, such as imaging, communications, chemical detection, photonic integrated circuits and astrophysics.

Acknowledgments. D. Sarker, P. P. Nakti, M. I. Tahmid, and M. A. Z. Mamun would like to thank the department of Electrical and Electronic Engineering (EEE), Shahjalal University of Science and Technology (SUST) for providing necessary facilities for the completion of the work. M.I. Tahmid and A. Zubair acknowledge the support and facilities received from the Department of EEE, Bangladesh University of Engineering and Technology (BUET).

Disclosures. The authors declare no conflict of interest.

Data availability. Data underlying the results presented in this paper are not publicly available at this time but may be obtained from the authors upon reasonable request.

Supplemental document. See Supplement 1 for supporting content.

References

1. Z. Song, J. Zhu, C. Zhu, Z. Yu, and Q. Liu, "Broadband cross polarization converter with unity efficiency for terahertz waves based on anisotropic dielectric meta-reflectarrays," Mater. Lett. **159**, 269–272 (2015).
2. Z. Song and J. Zhang, "Achieving broadband absorption and polarization conversion with a vanadium dioxide metasurface in the same terahertz frequencies," Opt. Express **28**(8), 12487–12497 (2020).
3. J. Wang, H. Tian, S. Li, L. Li, G. Wang, J. Gao, W. Guo, and Z. Zhou, "Efficient terahertz polarization conversion with hybrid coupling of chiral metamaterial," Opt. Lett. **45**(5), 1276–1279 (2020).
4. H. Zhang, Y. Liu, Z. Liu, X. Liu, G. Liu, G. Fu, J. Wang, and Y. Shen, "Multi-functional polarization conversion manipulation via graphene-based metasurface reflectors," Opt. Express **29**(1), 70–81 (2021).
5. M. Masyukov, A. Vozianova, A. Grebenchukov, K. Gubaidullina, A. Zaitsev, and M. Khodzitsky, "Optically tunable terahertz chiral metasurface based on multi-layered graphene," Sci. Rep. **10**(1), 3157 (2020).
6. R. Wang, J. Han, J. Liu, H. Tian, W. Sun, L. Li, and X. Chen, "Multi-foci metalens for terahertz polarization detection," Opt. Lett. **45**(13), 3506–3509 (2020).
7. L. Y. Deng, J. H. Teng, L. Zhang, Q. Y. Wu, H. Liu, X. H. Zhang, and S. J. Chua, "Extremely high extinction ratio terahertz broadband polarizer using bilayer subwavelength metal wire-grid structure," Appl. Phys. Lett. **101**(1), 011101 (2012).
8. Z. Huang, H. Park, E. P. J. Parrott, H. P. Chan, and E. Pickwell-MacPherson, "Robust thin-film wire-grid thz polarizer fabricated via a low-cost approach," IEEE Photonics Technol. Lett. **25**(1), 81–84 (2013).
9. H.-Y. Mao, L.-P. Xia, X.-H. Rao, H.-L. Cui, S.-J. Wang, Y.-S. Deng, D.-S. Wei, J. Shen, H.-M. Xu, and C.-L. Du, "A terahertz polarizer based on multilayer metal grating filled in polyimide film," IEEE Photonics J. **8**(1), 1–6 (2016).

Optics EXPRESS

10. L. Ren, C. L. Pint, T. Arikawa, K. Takeya, I. Kawayama, M. Tonouchi, R. H. Hauge, and J. Kono, "Broadband terahertz polarizers with ideal performance based on aligned carbon nanotube stacks," Nano Lett. **12**(2), 787–790 (2012).
11. L. Cong, W. Cao, Z. Tian, J. Gu, J. Han, and W. Zhang, "Manipulating polarization states of terahertz radiation using metamaterials," New J. Phys. **14**(11), 115013 (2012).
12. F. A. Juneghani, A. Zeidaabadi-Nezhad, and R. Safian, "Analysis of diffraction graphene gratings using the c-method and design of a terahertz polarizer," Prog. Electromagn. Res. M **65**, 175–186 (2018).
13. K. Meng, S. J. Park, L. H. Li, D. R. Bacon, L. Chen, K. Chae, J. Y. Park, A. D. Burnett, E. H. Linfield, A. G. Davies, and J. E. Cunningham, "Tunable broadband terahertz polarizer using graphene-metal hybrid metasurface," Opt. Express **27**(23), 33768–33778 (2019).
14. S. M. Raeis-Zadeh and S. Safavi-Naeini, "Application of graphene nanoholes as a terahertz polarizer," in *2015 IEEE International Symposium on Antennas and Propagation USNC/URSI National Radio Science Meeting*, (2015), pp. 1640–1641.
15. G. W. Hanson, "Dyadic green's functions and guided surface waves for a surface conductivity model of graphene," J. Appl. Phys. **103**(6), 064302 (2008).
16. C. Casiraghi, A. Hartschuh, E. Lidorikis, H. Qian, H. Harutyunyan, T. Gokus, K. S. Novoselov, and A. C. Ferrari, "Rayleigh imaging of graphene and graphene layers," Nano Lett. **7**(9), 2711–2717 (2007).
17. C. Li, Z. Xiao, W. Li, and H. Zou, "Tunable multiband band-stop filter based on graphene metamaterial in thz frequency," J. Electromagn. Waves Appl. **32**(18), 2481–2489 (2018).
18. L. Tai, D. Zhu, X. Liu, T. Yang, L. Wang, R. Wang, S. Jiang, Z. Chen, Z. Xu, and X. Li, "Direct growth of graphene on silicon by metal-free chemical vapor deposition," Nano-Micro Lett. **10**(2), 20 (2018).
19. A. N. Abbas, G. Liu, B. Liu, L. Zhang, H. Liu, D. Ohlberg, W. Wu, and C. Zhou, "Patterning, characterization, and chemical sensing applications of graphene nanoribbon arrays down to 5 nm using helium ion beam lithography," ACS Nano **8**(2), 1538–1546 (2014).
20. S. Shukla, S.-Y. Kang, and S. Saxena, "Synthesis and patterning of graphene: Strategies and prospects," Appl. Phys. Rev. **6**(2), 021311 (2019).
21. R. Yan, S. Arezoomandan, B. Sensale-Rodriguez, and H. G. Xing, "Exceptional terahertz wave modulation in graphene enhanced by frequency selective surfaces," ACS Photonics **3**(3), 315–323 (2016).
22. X. Zhao, J. Schalch, J. Zhang, H. R. Seren, G. Duan, R. D. Averitt, and X. Zhang, "Electromechanically tunable metasurface transmission waveplate at terahertz frequencies," Optica **5**(3), 303–310 (2018).
23. L. Cong, P. Pitchappa, C. Lee, and R. Singh, "Active phase transition via loss engineering in a terahertz mems metamaterial," Adv. Mater. **29**(26), 1700733 (2017).
24. L. Ju, B. Geng, J. Horng, C. Girit, M. Martin, Z. Hao, H. A. Bechtel, X. Liang, A. Zettl, Y. R. Shen, and F. Wang, "Graphene plasmonics for tunable terahertz metamaterials," Nat. Nanotechnol. **6**(10), 630–634 (2011).
25. W. Gao, J. Shu, C. Qiu, and Q. Xu, "Excitation of plasmonic waves in graphene by guided-mode resonances," ACS Nano **6**(9), 7806–7813 (2012).
26. L. A. Falkovsky, "Optical properties of graphene," J. Phys.: Conf. Ser. **129**, 012004 (2008).
27. D. D. Smith, N. N. Lepeshkin, A. Schweinsberg, G. Gehring, R. W. Boyd, Q.-H. Park, H. Chang, and D. J. Jackson, "Coupled-resonator-induced transparency in a fiber system," Opt. Commun. **264**(1), 163–168 (2006).
28. H.-J. Li, L.-L. Wang, J.-Q. Liu, Z.-R. Huang, B. Sun, and X. Zhai, "Investigation of the graphene based planar plasmonic filters," Appl. Phys. Lett. **103**(21), 211104 (2013).
29. L. Zhu, F.-Y. Meng, L. Dong, Q. Wu, B.-J. Che, J. Gao, J.-H. Fu, K. Zhang, and G.-H. Yang, "Magnetic metamaterial analog of electromagnetically induced transparency and absorption," J. Appl. Phys. **117**(17), 17D146 (2015).
30. S. Zhang, D. A. Genov, Y. Wang, M. Liu, and X. Zhang, "Plasmon-induced transparency in metamaterials," Phys. Rev. Lett. **101**(4), 047401 (2008).
31. S. khazaee and N. Granpayeh, "Tunable multiple plasmon induced transparencies in parallel graphene sheets and its applications," Opt. Commun. **406**, 199–204 (2018).
32. X. Zhang, Z. Liu, Z. Zhang, E. Gao, X. Luo, F. Zhou, H. Li, and Z. Yi, "Polarization-sensitive triple plasmon-induced transparency with synchronous and asynchronous switching based on monolayer graphene metamaterials," Opt. Express **28**(24), 36771–36783 (2020).
33. A. Zubair, D. E. Tsentalovich, C. C. Young, M. S. Heimbeck, H. O. Everitt, M. Pasquali, and J. Kono, "Carbon nanotube fiber terahertz polarizer," Appl. Phys. Lett. **108**(14), 141107 (2016).
34. Q. Bao, H. Zhang, B. Wang, Z. Ni, C. H. Y. X. Lim, Y. Wang, D. Y. Tang, and K. P. Loh, "Broadband graphene polarizer," Nat. Photonics **5**(7), 411–415 (2011).
35. C. Pei, L. Yang, G. Wang, Y. Wang, X. Jiang, Y. Hao, Y. Li, and J. Yang, "Broadband graphene/glass hybrid waveguide polarizer," IEEE Photonics Technol. Lett. **27**(9), 927–930 (2015).